Journal of Physiology (2002), **538.2**, *pp.* 447–463
DOI: 10.1013/jphysiol.2001.013051

www.jphysiol.org

Analysis of whole-cell currents by patch clamp of guinea-pig myenteric neurones in intact ganglia

François Rugiero, Maurice Gola, Wolf A. A. Kunze *, Jean-Claude Reynaud, John B. Furness * and Nadine Clerc

*Laboratoire 'Intégration des Informations Sensorielles' (ITIS), CNRS, Bâtiment LNB, No. 31, Chemin Joseph Aiguier, 13402 Marseille Cedex 20, France and *Department of Anatomy and Cell Biology, University of Melbourne, Parkville, VIC 3010, Australia*

Whole-cell patch-clamp recordings taken from guinea-pig duodenal myenteric neurones within intact ganglia were used to determine the properties of S and AH neurones. Major currents that determine the states of AH neurones were identified and quantified. S neurones had resting potentials of −47 ± 6 mV and input resistances (R_{in}) of 713 ± 49 MΩ at voltages ranging from −90 to −40 mV. At more negative levels, activation of a time-independent, caesium-sensitive, inward-rectifier current (I_{Kir}) decreased R_{in} to 103 ± 10 MΩ. AH neurones had resting potentials of −57 ± 4 mV and R_{in} was 502 ± 27 MΩ. R_{in} fell to 194 ± 16 MΩ upon hyperpolarization. This decrease was attributable mainly to the activation of a cationic h current, I_h, and to I_{Kir}. Resting potential and R_{in} exhibited a low sensitivity to changes in $[K^+]_o$ in both AH and S neurones. This indicates that both cells have a low background K^+ permeability. The cationic current, I_h, contributed about 20 % to the resting conductance of AH neurones. It had a half-activation voltage of −72 ± 2 mV, and a voltage sensitivity of 8.2 ± 0.7 mV per e-fold change. I_h has relatively fast, voltage-dependent kinetics, with on and off time constants in the range of 50–350 ms. AH neurones had a previously undescribed, low threshold, slowly inactivating, sodium-dependent current that was poorly sensitive to TTX. In AH neurones, the post-action-potential slow hyperpolarizing current, I_{AHP}, displayed large variation from cell to cell. I_{AHP} appeared to be highly Ca^{2+} sensitive, since its activation with either membrane depolarization or caffeine (1 mM) was not prevented by perfusing the cell with 10 mM BAPTA. We determined the identity of the Ca^{2+} channels linked to I_{AHP}. Action potentials of AH neurones that were elongated by TEA (10 mM) were similarly shortened and I_{AHP} was suppressed with each of the three ω-conotoxins GVIA, MVIIA and MVIIC (0.3–0.5 μM), but not with ω-agatoxin IVA (0.2 μM). There was no additivity between the effects of the three conotoxins, which indicates the presence of N- but not of P/Q-type Ca^{2+} channels. A residual Ca^{2+} current, resistant to all toxins, but blocked by 0.5 mM Cd^{2+}, could not generate I_{AHP}. This patch-clamp study, performed on intact ganglia, demonstrates that the AH neurones of the guinea-pig duodenum are under the control of four major currents, I_{AHP}, I_h, an N-type Ca^{2+} current and a slowly inactivating Na^+ current.

(Resubmitted 27 July 2001; accepted after revision 18 October 2001)
Corresponding author M. Gola: Laboratoire Intégration des Informations Sensorielles (ITIS), CNRS, Bâtiment LNB, 31 Chemin Joseph Aiguier, 13402 Marseille Cedex 20, France. Email: gola@lnb.cnrs-mrs.fr

The aim of the present paper was to determine the electrotonic properties of myenteric neurones, using patch-clamp recording from non-dissociated myenteric neurones, with emphasis on the identification and quantitation of the ionic currents that modulate the resting membrane potential of AH neurones. Recordings were made with a technique we have recently developed for patch-clamp recording from intact ganglia (Kunze *et al.* 2000).

The electrophysiological properties of myenteric neurones in intact ganglia from the small intestine of the guinea-pig have been investigated previously by intracellular recordings in myenteric plexus/longitudinal muscle preparations. The first intracellular recording studies were performed using duodenal (Hirst *et al.* 1974) and ileal tissue (Nishi & North, 1973). In both of these parts of the intestine, the studies separated the myenteric neurones into two groups, S and AH neurones, terms that were introduced in 1974 for duodenal neurones (Hirst *et al.* 1974). S neurones were so named because they received prominent fast synaptic inputs, while AH neurones did not. AH neurones were so named because the action potential is followed by a long-lasting after-hyperpolarization (AHP). It was later demonstrated that both cell types receive slow EPSPs (Wood & Meyer, 1978; Johnson *et al.* 1980, 1981; Bornstein *et al.* 1984).

Correlations between electrophysiological characteristics and cell morphology have been made by intracellular recording using micropipettes filled with fluorescent dyes (e.g. biocytin or neurobiotin) in the ileum (Hodgkiss & Lees, 1983; Iyer *et al.* 1988; Bornstein *et al.* 1991) and the duodenum (Clerc *et al.* 1998). These and other studies showed that AH neurones comprise a single population with Dogiel type II morphology, and were later shown to be sensory, while S neurones were uniaxonal neurones (Bornstein *et al.* 1994). Motor neurones to muscle, secretomotor neurones and interneurones, of which there are four types in the myenteric ganglia of the guinea-pig small intestine (Costa *et al.* 1996; Furness, 2000) are S neurones.

At the present time, two different ionic currents are known to modulate the resting membrane potential of AH neurones directly: a K^+ inward rectifier current (I_{Kir}), which has been described in both AH and S neurones, and a slow AHP current (I_{AHP}), which is typical of the AH neurones. A cationic current activated by hyperpolarization (I_h) has been described in AH neurones (Galligan *et al.* 1990) and in a subpopulation of S neurones, the filamentous interneurones in the ileum (Song *et al.* 1997). This current has been shown to contribute to the membrane potential in other types of neurone (Doan & Kunze, 1999). In addition, a high-voltage-activated (HVA) Ca^{2+} current is activated during the action potential of AH neurones (Hirst *et al.* 1974) and less prominently in some filamentous interneurones (Song *et al.* 1997; Clerc *et al.* 1998). In AH neurones, but not in the filamentous interneurones of the duodenum (Clerc *et al.* 1998), this Ca^{2+} current indirectly controls the membrane potential by activating the I_{AHP}.

Although described in a sharp electrode study (Galligan *et al.* 1990), the I_h has not been recognized in a recent patch electrode study of dissociated myenteric neurones (Zholos *et al.* 1999) in which only I_{Kir} was identified. We have found both currents in AH neurones and, because I_h is known to activate at potentials between −45 and −60 mV in other neuronal types (Pape, 1996), we investigated its possible contribution to the resting membrane potential. We have also detected a slowly inactivating Na^+ current that was poorly sensitive to TTX and might modulate the resting membrane potential of these neurones.

The activation of I_{AHP} is triggered by the opening of HVA Ca^{2+} channels whose identity is controversial (Baidan *et al.* 1992*b*; Furness *et al.* 1998; Starodub & Wood, 1999; Vogalis *et al.* 2001). Intracellular studies (Kunze *et al.* 1994; Furness *et al.* 1998) as well as a recent patch-clamp study (Vogalis *et al.* 2001) suggest that N-type but not L-type channels are involved, because the hump on the falling phase of the action potential of AH neurones persisted in the presence of nicardipine, but was attenuated by the N-type Ca^{2+} channel blocker *ω*-conotoxin GVIA (*ω*-CgTX GVIA). According to patch-clamp studies performed in dissociated myenteric neurones, the HVA Ca^{2+} current is suppressed by this conotoxin (Baidan *et al.* 1992*b*). In the case of rat myenteric neurones in cell culture, both L- and N-type Ca^{2+} channels contributed to the HVA Ca^{2+} current (Franklin & Willard, 1993). However, on the basis of the effect of *ω*-CgTX MVIIC, which is a blocker of P- and Q-type Ca^{2+} channels, and to a lesser extent of N-type channels (Uchitel, 1997), Starodub & Wood (1999) concluded that AH neurones express mainly P/Q-type channels. Therefore, we performed a systematic pharmacological investigation to characterize the HVA Ca^{2+} channel types. In addition, we evaluated the sensitivity of I_{AHP} to $[Ca^{2+}]_i$.

Some of the results presented here have been published in abstract form (Clerc *et al.* 2000).

METHODS

Preparation

Patch-clamp experiments were carried out on non-dissociated neurones, in intact ganglia of the myenteric plexus. All experiments were performed using 2- to 3-cm-long segments of the proximal duodenum excised from guinea-pigs (150–400 g) after they were stunned and decapitated. Guinea-pigs were Hartley strain from the inbred colony at the IFR 'Sciences du Cerveau', CNRS, Marseilles. All procedures were approved by the French Ministry of Agriculture and Fisheries and were in agreement with the European Communities Council Directive 86/609/EEC. The segments of duodenum were placed in a recording dish that had a transparent base and was filled with oxygenated Krebs solution (see below), which was kept at room temperature during dissection, but which was heated to 34 °C during recording. The myenteric plexus was exposed by dissecting away the mucosa, submucosal plexus and circular muscle, and the preparation was mounted in a transparent recording dish on the stage of an inverted microscope. The surface of one ganglion was exposed to 0.01–0.02 % protease type XIV (Sigma, St Louis, MO, USA) in physiological saline, and the upper surfaces of neurones were cleaned by sweeping with a hair over the ganglion (Gola & Niel, 1993; Kunze *et al.* 2000).

Electrophysiological recordings

Membrane current and voltage were measured with a List EPC7 amplifier using the whole-cell patch-clamp technique. Borosilicate glass capillaries were pulled in four steps with a P 87 Flaming-Brown puller (Sutter Instruments) to obtain micropipettes with a resistance of about 2–4 MΩ. A fairly strong pressure (60–80 hPa) was applied to the pipette in order to eliminate residual matter adhering to the nerve cell surface. The pressure was released when the pipette contacted the membrane and suction (10–20 hPa) was applied to form a gigaseal. The whole-cell configuration was achieved by subjecting the patch membrane to a slight suction. Current and voltage traces were low-pass filtered at 5 kHz, then digitized at 44 kHz, stored on a computer and subsequently analysed. Quasi-steady-state *I–V* relationships were obtained using slow voltage ramps rather than voltage steps. The voltage error due to uncompensated series resistance ranged from 1 to 3 mV. Values are expressed as means ± S.D. or S.E.M. (specified in the text).

Solutions

If not otherwise specified in the text and figure legends, solutions were as follows: Krebs solution (mM): 118 NaCl, 4.8 KCl, 1.0 NaH_2PO_4, 2.5 $CaCl_2$, 1 $MgSO_4$, 25 $NaHCO_3$ and 11.1 D-glucose bubbled with a 95 % O_2–5 % CO_2 gas mixture (pH 7.4). Hyoscine (1 μM) and nicardipine (3 μM) were added to the superfusate to block spontaneous muscle movement. Ionic substitutions were achieved by isosmotically changing the $[Na^+]$ or $[K^+]$ of the following saline (mM): 145 NaCl, 4.8 KCl, 2.5 $CaCl_2$, 1 $MgSO_4$ and 10 Hepes. Na^+ was replaced with either *N*-methyl D-glucamine (NMDG) or choline. The Hepes saline was also used when Cd^{2+} and Ba^{2+} were added. The patch pipettes were filled with a solution consisting of (mM): KCl 140, NaCl 4, $CaCl_2$ 1, $MgCl_2$ 2, Hepes 10, EGTA 2, GTP 0.2, (pH 7.3). Any changes in this standard filling saline are indicated in the text.

Cells were continuously superfused with the external solution (2 ml min^{-1}). Fast local applications of drugs were performed by gravity from several reservoirs connected to a common outlet positioned as near as possible to the cell investigated. The solution to be applied was selected by activating solenoid valves. Salts were purchased from Prolabo (Lyon, France); the ω-conotoxins MVIIA, MVIIC and GVIA were from Latoxan (Valence, France), and ω-agatoxin IVA was from Peptides International (Louisville, KY, USA). All of the other chemicals were from Sigma (St Louis, MO, USA).

Criteria for identifying AH and S neurones

Some of the superficial neurones in the cleaned ganglia remained covered with glial cells, collagen fibres or basal lamina. Only recordings in which the seal resistance was larger than 5 GΩ were utilized. In a representative series of 20 experiments, the mean number of patch-clamped cells per ganglion was: glial cells, 0.65 (range 0–4); AH neurones, 2.6 (range 0–5); S neurones, 1.1 (range 0–4).

AH neurones had each of the following electrophysiological characteristics: a large action potential with a characteristic hump on the repolarizing phase (Fig. 1*Aa*), a long-lasting AHP (Fig. 12*B*) and a sag in the voltage response to hyperpolarizing current pulses (Kunze *et al.* 2000; see Fig. 4*A*). S neurones responded with an exponential hyperpolarization to small inward current pulses (see Fig. 2*A*). Their action potentials had no hump on the falling phase and were not followed by a long-lasting AHP.

AH neurones were also fired antidromically by applying a single electric shock (0.1 ms, 8–25 V) to one of the nerve fibre bundles joining the ganglion containing the nerve cell (Fig. 1*Ab*). The antidromic origin of the evoked action potential was confirmed by performing a collision test (not illustrated). Single electric shocks never induced any fast EPSP in AH neurones. In the case of S neurones, nerve stimulation generally resulted in an action potential superimposed on a fast excitatory synaptic potential. The synaptic potential was unmasked by moderately hyperpolarizing the cell (Fig. 1*Bb*).

RESULTS

Data were collected from 92 ganglia. In addition to the currents investigated in detail here, both S and AH neurones had a TTX-sensitive Na^+ current (I_{NaT}), which participated in the generation of the action potential, an outwardly rectifying voltage-dependent and TEA-sensitive K^+ current, and a transient A-type K^+ current (Baidan *et al.* 1992*a*; Zholos *et al.* 1999; Hanani *et al.* 2000; Starodub & Wood, 2000; Vogalis *et al.* 2000). In both AH and S neurones, the inactivation of the A current was fast, 19–25 ms ($n = 9$) at −50 mV. Its voltage dependence (fitted to Boltzmann functions) had a sensitivity of 6.2 ± 0.9 mV, and a voltage at half activation of −78 ± 5 mV. These values are similar to those measured in cultured AH neurones (Vogalis *et al.* 2000). Therefore, at voltages positive to −60 mV, the A current played a limited role in shaping the action potential of AH and S neurones.

Action potential parameters

Immediately after the patch was disrupted, AH neurones had a resting potential of −57 ± 4 mV (mean ± S.D.), range −48 to −69 mV ($n = 61$). S neurones had a smaller resting potential to AH neurones, −47 ± 6 mV, range −36 to −64 mV ($n = 35$). The action potential was triggered with a 10-ms-duration depolarizing current pulse, the amplitude of which was adjusted so that the action potential was evoked after the pulse (Fig. 1*Aa* and *Ba*).

Action potential parameters, collected from 71 AH neurones investigated using the standard pipette saline, were (mean ± S.D.): overshoot, 46 ± 6 mV; maximum hyperpolarization of the fast AHP, −70 ± 5 mV; peak-to-peak amplitude, 115 ± 8 mV (amplitude from membrane potential, 102 ± 5 mV); duration (measured at half-amplitude) 2.8 ± 0.2 ms. The distribution of the AH action potential parameters are given in Fig. 1*D*–*G* (filled columns). The corresponding values for S neurones ($n = 35$) were: overshoot, 27 ± 9 mV; fast AHP, −62 ± 6 mV; peak-to-peak amplitude, 88 ± 12 mV (amplitude from membrane potential, 73 ± 12 mV); action potential duration, 2.2 ± 0.8 mV. The distribution of the S action potential parameters is given in Fig. 1*D*–*G* (open columns).

The relatively low action potential amplitude of S neurones was for a large part accounted for by the low resting polarization of these cells. When S neurones were progressively hyperpolarized by injecting an increasing inward current, the action potential overshoot increased and reached values comparable to those of AH neurones. The relationship between the cell polarization and the action potential characteristics of the S and AH populations shown in Fig. 1*D*–*F* are given in Fig. 1*Ha* and *Hb*, respectively.

Electrotonic properties of S neurones

Electrotonic properties were determined in either current-clamp or voltage-clamp conditions. The input resistance (R_{in}) was measured by injecting 0.5 s hyperpolarizing current pulses of increasing amplitude (from 20 to 120–160 pA). S neurones responded by a large hyperpolarization that tended to saturate at large current intensity (Fig. 2*A*). The corresponding *I*–*V* plot showed

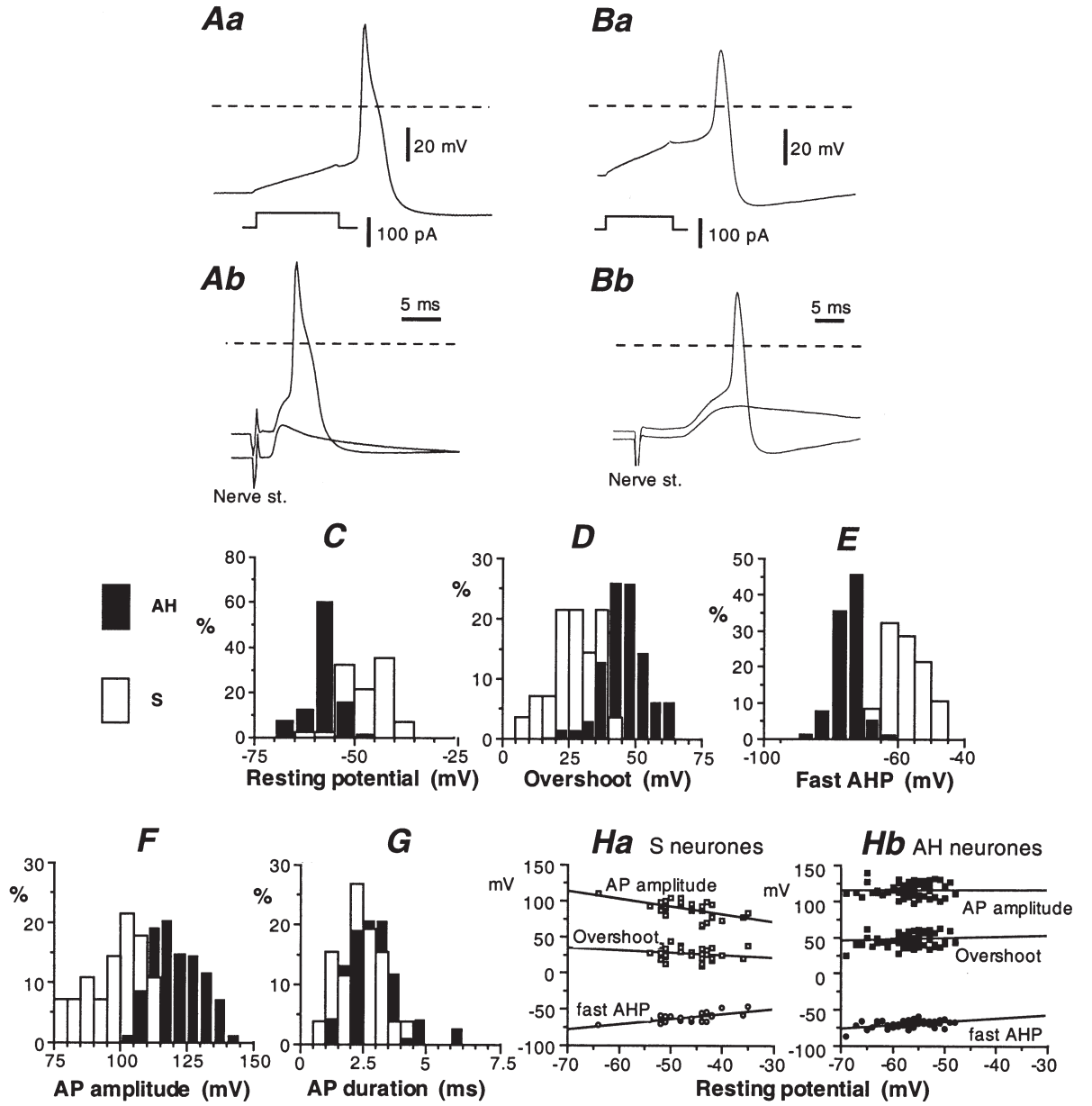

Figure 1. Action potential characteristics of AH and S neurones

A and *B*, action potentials triggered by stimulating an AH neurone (*Aa*) and an S neurone (*Ba*) with an intracellular current pulse (lower trace in *Aa* and *Ba*) or applying an electrical shock (nerve stimulation, 0.1 ms, 10–20 V) to one of the nerves connected to the ganglion (*Ab* and *Bb*). In *Ab*, the action potential of the AH neurone was antidromically evoked. A non-invading electrotonic potential ('A spike'; lower trace in *Ab*) was revealed by hyperpolarizing the cell. The nerve stimulation in *Bb* evoked a fast EPSP (lower trace) that was large enough to trigger an overshooting action potential in an S neurone. Hyperpolarization revealed the synaptic potential without the superimposed action potential (lower trace). Dashed lines show the 0 mV level. *C*, distribution of the resting potential of AH (filled columns) and S neurones (open columns). The resting potential was measured within 30 s after patch rupture and is not corrected for electrode tip potential. This histogram was derived from the results of 71 AH neurones and 38 S neurones. *D*–*G*, distribution of the action potential characteristics of AH neurones (filled columns) and S neurones (open columns). Same population as in *C*. The peak-to-peak action potential amplitude (*F*) was measured from the overshoot (*D*) to the after-hyperpolarization (AHP) immediately following the action potential repolarization (*E*). The action potential duration (*G*) was measured at half amplitude (~ −20 mV). *Ha* and *Hb*, dependence of the action potential characteristics of S and AH neurones on the resting potential. In *C*–*G*, results are expressed as the percentage (%) of the cell population by bin (5 mV in *C*–*F*, 0.5 ms in *G*).

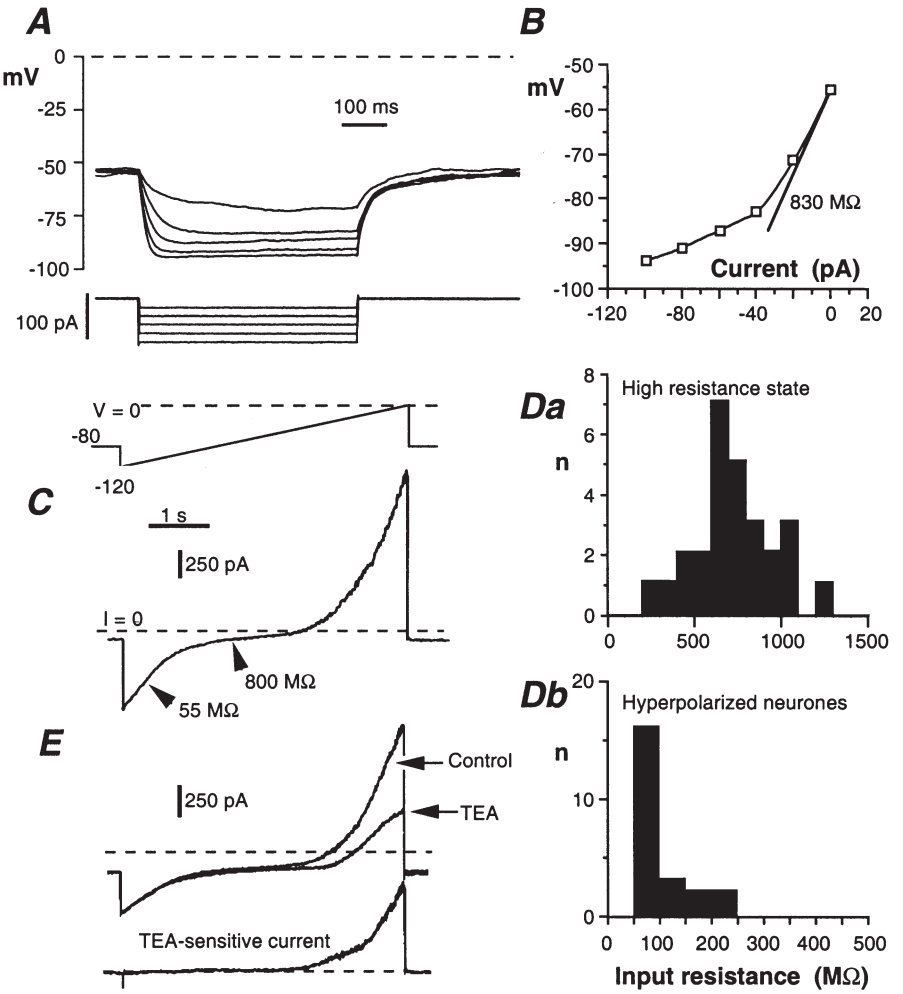

Figure 2. Input resistance of S neurones

A, response of an S neurone to 0.5 s hyperpolarizing current pulses incremented by 20 pA. *B*, corresponding *I–V* plot measured at the end of the current pulse. Input resistance (R_{in}) at rest is given by the slope of the straight line. Reduced R_{in} at hyperpolarized potentials is due to the presence of an inward rectifier. *C*, S neurone subjected to a slowly rising (24 mV s^{-1}) voltage ramp (voltage-clamp conditions) from −120 to 0 mV. S neurones had a high R_{in} between −90 and −40 mV. The impedance was considerably reduced by the activation of an inwardly rectifying K^+ current at $V < -90$ mV and by a delayed rectifier at $V > -40$ mV. *D*, distribution of R_{in} of S neurones in the high-resistance state (*Da*) and upon activation of the inwardly rectifying current (*Db*). *E*, effect of TEA (10 mM) on the *I–V* curve. Same voltage programme as in *C*. Lower trace, difference current revealing the delayed rectifier.

that the S neurones have a high R_{in} at voltages negative to −40 mV and that R_{in} was considerably reduced at voltages negative to −90 mV (Fig. 2*B*). The time constant ($\tau = 32 \pm 4$ ms, $n = 18$) of the exponential change in voltage in response to small (10 to −20 pA) current pulses yielded a membrane capacitance of 48 ± 3 pF.

The quasi steady-state *I–V* relationship obtained with slowly rising voltage ramps from −120 to 0 or +20 mV was S-shaped (Fig. 2*C*). From −90 to −40 mV, S neurones had a high R_{in} (713 ± 49 MΩ, $n = 27$; Fig. 2*Da*). On both sides of this range the membrane conductance increased. The conductance increase at $V > -40$ mV resulted from the

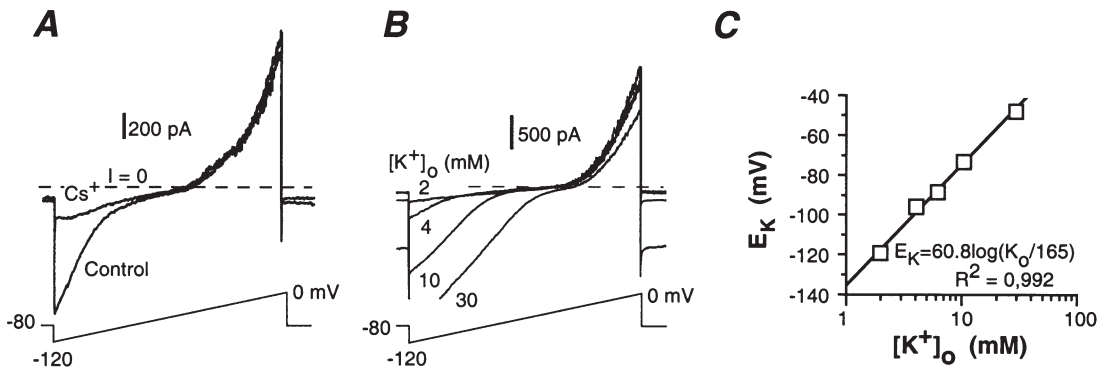

Figure 3. Properties of the inward rectifier of S neurones

A, current response to depolarizing voltage-ramps in an S neurone in physiological saline (control) and in the presence of 2 mM extracellular Cs^+. Cs^+ abolished the increase in inward current at $V < -90$ mV. *B*, increase of the inwardly rectifying current by changing the $[K^+]_o$ from 2 to 30 mM. *C*, plot of the threshold of the inwardly rectifying current, identified as the K^+ reversal potential (E_K), *versus* $[K^+]_o$. Data are from the experiment illustrated in *B*.

activation of a TEA-sensitive delayed rectifier (Fig. 2*E*). The increase at $V < -90$ mV was due to the activation of a time-independent inwardly rectifying K^+ current, I_{Kir}. The inward rectifier decreased R_{in} to 103 ± 10 MΩ ($n = 23$; Fig. 2*Db*). A prominent inward rectifier was present in 30 out of 32 S neurones. The I_{Kir} conductance, obtained by subtracting the conductance in the high-resistance state from that with I_{Kir} activated, had a mean value (± S.E.M.) of 9.5 ± 0.9 nS (range 3.1–17.4 nS).

The inward rectifier was blocked by adding 1–2 mM Cs^+ (Fig. 3*A*) to the bath saline. As expected for an inward rectifier, the inward current was strongly dependent on the $[K^+]_o$ of the bath saline for both its conductance and location on the voltage axis (Fig. 3*B*). The voltage at which this current vanished followed perfectly the change in K^+ driving force derived from the Nernst relationship (Fig. 3*C*).

The high-resistance state was poorly dependent on $[K^+]_o$. In the experiment illustrated in Fig. 3*B*, the resting potential changed from −48 to −40 mV when $[K^+]_o$ was increased from 2 to 30 mM. This voltage shift was much smaller than the value predicted (i.e. $\Delta V = 68$ mV) for selective K^+

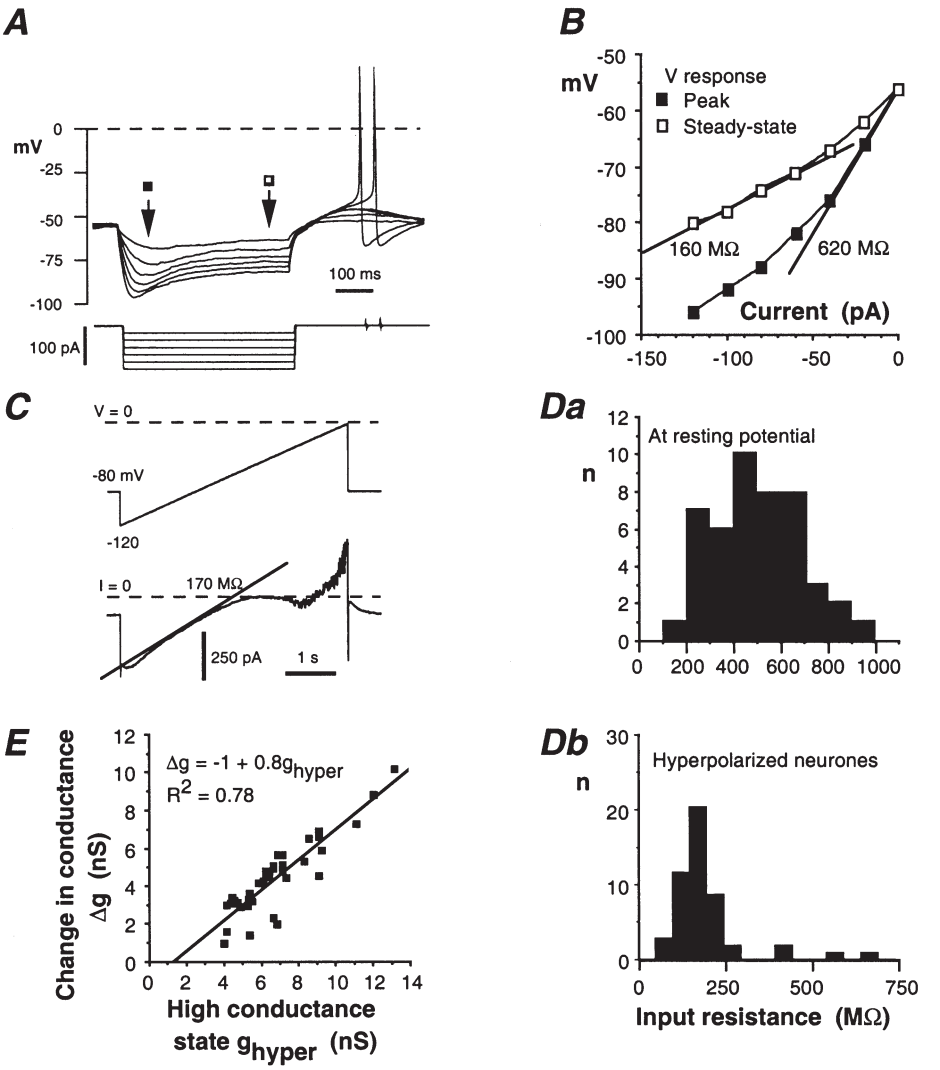

Figure 4. R_{in} of AH neurones

A, response of an AH neurone to 0.5 s hyperpolarizing current pulses incremented by 20 pA. *B*, *I–V* plot for the cell illustrated in *A*. Filled squares: relationship prior to I_h activation; open squares: relationship in presence of I_h. Slope resistances are measured from the straight lines shown on the figure. *C*, same neurone subjected to a slowly (24 mV s^{-1}) rising voltage-ramp (voltage-clamp conditions) from −120 to 0 mV. The slope of the current trace at voltages positive to −90 mV corresponded to a R_{in} of 170 MΩ. *D*, distribution of the R_{in} in AH neurones. *Da*, neurones at the resting potential; R_{in} determined as shown in *B* (filled squares). *Db*, R_{in} upon activation of the h current (open squares in *B*). *E*, relationship between the high conductance state g_{hyper} (nS) in hyperpolarized neurones (data are from *Db*) and the increase in conductance (Δg) that occurred when AH neurones were hyperpolarized from the resting level.

conductance by the Nernst equation (Fig. 3*C*). This means that S neurones have a low resting K^+ permeability.

Electrotonic properties of AH neurones

The electrotonic properties of AH neurones were determined as described for S neurones. The voltage response to hyperpolarizing current displayed a pronounced sag, even with small (20 pA) current pulses (Fig. 4*A*). This sag can be ascribed to the activation of a cationic h-type current (see below). R_{in} was obtained by plotting the peak of the voltage response *versus* injected current, and by taking the slope of the *I–V* curve extrapolated to zero current (Fig. 4*B*). This procedure avoided underestimation of R_{in} due to the activation of I_h during current injection. Activation of I_h, already present with currents as small as 20 pA, produced a large decrease in R_{in} when the current pulse was increased (open squares in Fig. 4*B*). This effect was quantified by subjecting the neurones to slowly rising voltage ramps (20–25 mV s^{-1}) from −120 mV (I_h fully activated) to 0 mV, and by measuring the slope conductance at voltages positive to −90 mV (Fig. 4*C*). Voltages more negative than −90 mV activated an inward rectifier that was partly masked by the large I_h. This procedure gave values similar to those derived from the extrapolated steady-state *I–V* plot shown in Fig. 4*B* (170 MΩ compared to 160 MΩ).

The R_{in} of AH neurones displayed large variations, from 195 to 926 MΩ, with a mean ± S.E.M. of 502 ± 27 MΩ ($n = 47$; Fig. 4*Da*). In 53 out of 58 AH neurones, R_{in} fell upon activation of I_h (Fig. 4*Db*), on average to 194 ± 16 MΩ. Some of the variation of R_{in} might be attributable to the seal quality or, more probably, from variation in the level of I_h expression. There was indeed a strong correlation between the increase in input conductance (Δg) upon hyperpolarization (mostly attributable to I_h activation) and the level reached in the high-conductance state (Fig. 4*E*).

The cell capacitance was derived from the time constant of the initial exponential voltage change in response to small current pulses (5–10 pA). Its mean value was 61 ± 4 pF ($n = 18$).

Changing $[K^+]_o$ from 2 to 30 mM increased the inwardly rectifying current as well as I_h, but did not significantly alter the slope conductance between −60 and −40 mV (Fig. 5*A*). In eight neurones, the mean resting potential changed from −58 mV at 2 mM $[K^+]_o$ to −33 mV at 30 mM $[K^+]_o$, which was smaller than the value predicted for selective K^+ conductance by the Nernst equation (see above; Fig. 5*B*) as well as the value measured when a pure K^+ conductance (I_{AHP}) is activated (Fig. 5*B*). Therefore, like S neurones, AH neurones exhibited a low permeability to K^+ at rest.

Hyperpolarization-activated cationic h current in AH neurones

The sag in the voltage response of AH neurones to current pulses is characteristic of the presence of an h-type current. This current was not present in S neurones. The properties of I_h were determined in voltage-clamped neurones held between −40 and −50 mV and subjected to 1 s hyperpolarizing voltage pulses (Fig. 6*A*). This current had a null-current voltage (E_h) close to −40 mV. The maximal conductance (g_h) reached at large polarization and the steady-state activation (a_∞) were determined from the amplitude of the slowly activating h current, as shown in Fig. 6*A*, and the driving force $V - E_h$: $I_h = g_h \times a_\infty \times (V - E_h)$.

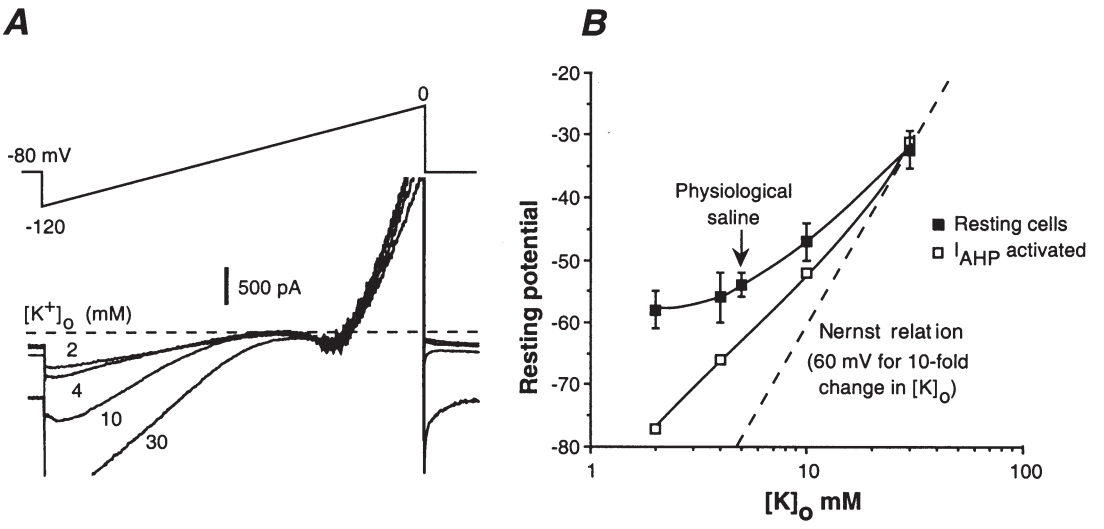

Figure 5. Sensitivity of AH neurones to changes in $[K^+]_o$

A, increase in I_{Kir} and I_h with elevated $[K^+]_o$ (same conditions as in Fig. 3*B*). *B*, effects of changes in $[K^+]_o$ on the membrane potential of AH neurones at rest (filled squares, $n = 7$) and when I_{AHP} is activated (open squares) compared to the theoritical changes for a K^+ conductance according to the Nernst relationship (dotted line). Open squares, example of the AHP sensitivity to changes in $[K^+]_o$.

Except for a few neurones in which I_h was poorly present (5 of 58), most AH neurones had a prominent h conductance ranging from 2 to 8 nS (see below; Fig. 6*B*). The activation, a_∞, was well approximated by the following equation:

$$a_\infty = 1/(1 + \exp((V - V_0)/p))$$

(Fig. 6*C*) with the half-activation voltage being $V_0 = -72 \pm 2$ mV ($n = 12$), and the voltage sensitivity factor being $p = 8.2 \pm 0.7$ mV, for an e-fold change in g_h.

The h current developed almost monoexponentially with a time constant (τ_h) that decreased at large polarizations. The voltage dependence of τ_h was determined from both activation and deactivation time courses. The τ_h–V curve was bell-shaped (Fig. 6*D*). It was approximated by the following relationship:

$$\tau_h = a + b \times [\exp((V - V_0)/r) + \exp(-(V - V_0)/r)]^{-1}.$$

V_0 had the value determined above; $a = 56 \pm 8$ ms; $b = 537 \pm 49$ ms; $r = 11.9 \pm 1.8$ mV.

The activation curve shows that I_h was activated by about 20 % (see Fig. 6*C*) at the mean resting potential of AH neurones (−57 mV). The maximal h conductance (g_h) reached at large polarization was 2.85 ± 0.22 nS ($n = 55$), which means that I_h contributed 0.57 nS to the input conductance of resting AH neurones. This input conductance was 1.99 ± 0.11 nS. Therefore, the remaining

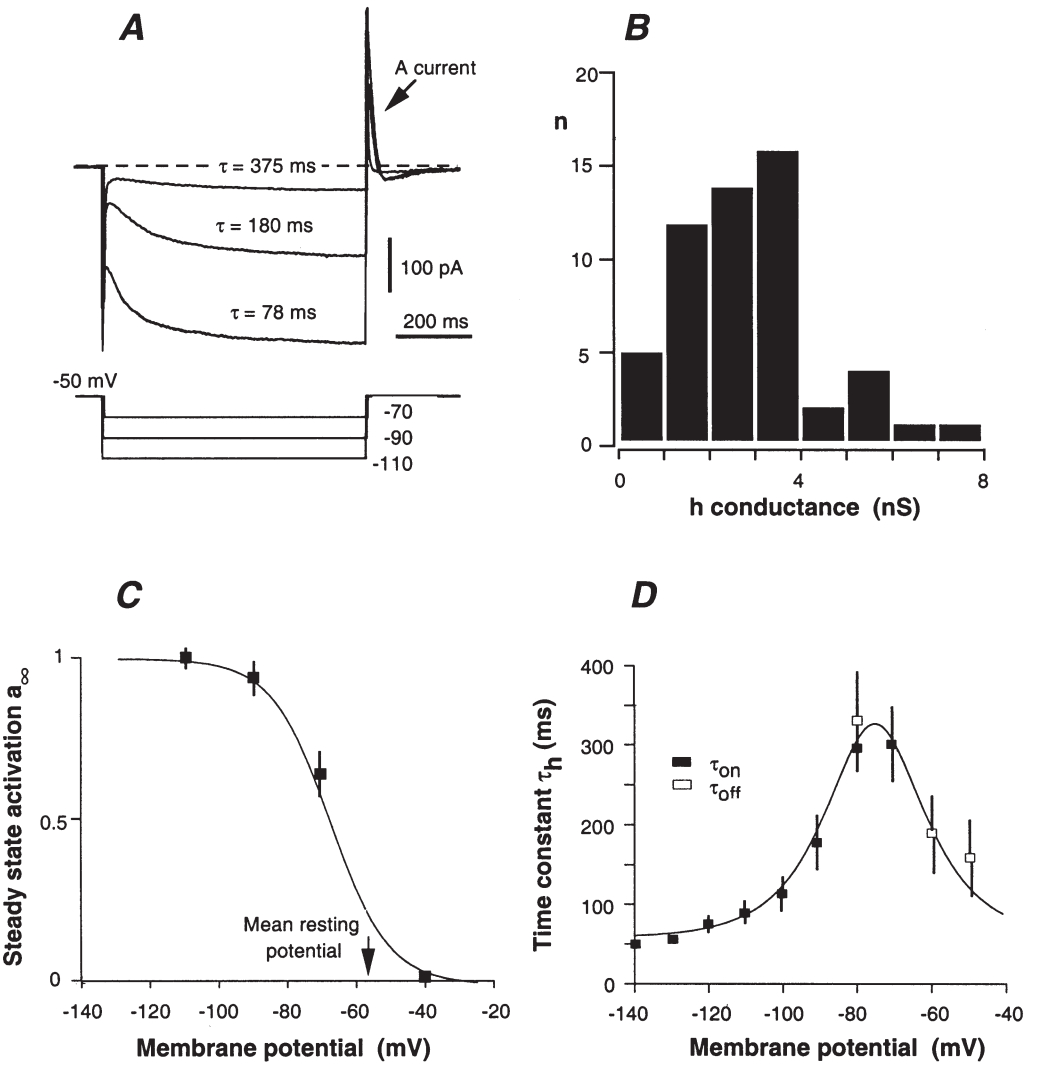

Figure 6. Properties of the cationic h current (I_h) of AH neurones

A, current response of an AH neurone to 1 s hyperpolarizing voltage pulses applied from −50 mV. Note the transient activation of a fast A-type K^+ current immediately after the pulse. *B*, distribution of the maximal h conductance in 58 AH neurones. The h conductance was evaluated from the amplitude of the steady-state I_h and the I_h reversal potential, $E_h = -40$ mV. *C*, steady-state activation, a_∞, of I_h. Data are from seven AH neurones. The curve was drawn according to the equation given in the text. *D*, voltage dependence of the time constant, τ_h of I_h changes. Data are from 14 AH neurones. τ_h was determined by fitting the current change to exponential curves during the hyperpolarizing voltage pulse (τ_{on}) and after the current pulse (τ_{off}). The continuous curve was drawn according to the equation given in the text.

background conductance, including the K^+ conductance, would be about 1.42 nS. This estimate is supported by the following data. Cationic h currents are blocked by $[Cs^+]_o$ (Pape, 1996). Adding 2 mM Cs^+ to the bath saline fully and reversibly blocked I_h in AH neurones (Fig. 7*Aa*). In these conditions, the *I–V* relationship in the −100 to −40 mV range became almost linear, with a slope of 1.49 ± 0.13 nS ($n = 14$; Fig. 7*Ab* and *Ba*). Note that Cs^+ also blocked I_{Kir}, which is visible at voltages negative to −100 mV in the instantaneous *I–V* plot shown in Fig. 7*Ab* (control curve at $t = 0$). As in S neurones, I_{Kir} was instantaneously activated, and was reversibly blocked by adding 2 mM Ba^{2+}, while I_h persisted (Fig. 7*C*). The caesium-sensitive current in the voltage range −100 to −20 mV was divided by the cationic driving force ($V - E_h$), resulting in the activation curve shown in Fig. 7*Bb*. This method yielded results similar to that described above. Under current-clamp conditions, caesium-treated AH neurones responded to hyperpolarizing current pulses by an exponential hyperpolarization far larger than in control conditions, indicating an increase in R_{in}, which reached 0.7 GΩ (Fig. 7*D*). However, Cs^+ treatment of neurones did not cause any change in resting membrane potential.

Low-threshold sodium-dependent current in AH neurones

The quasi-steady-state *I–V* curve of AH neurones displayed a more or less pronounced inflexion at voltages positive to the resting potential (see Figs 4*C* and 5*A*), or even a net

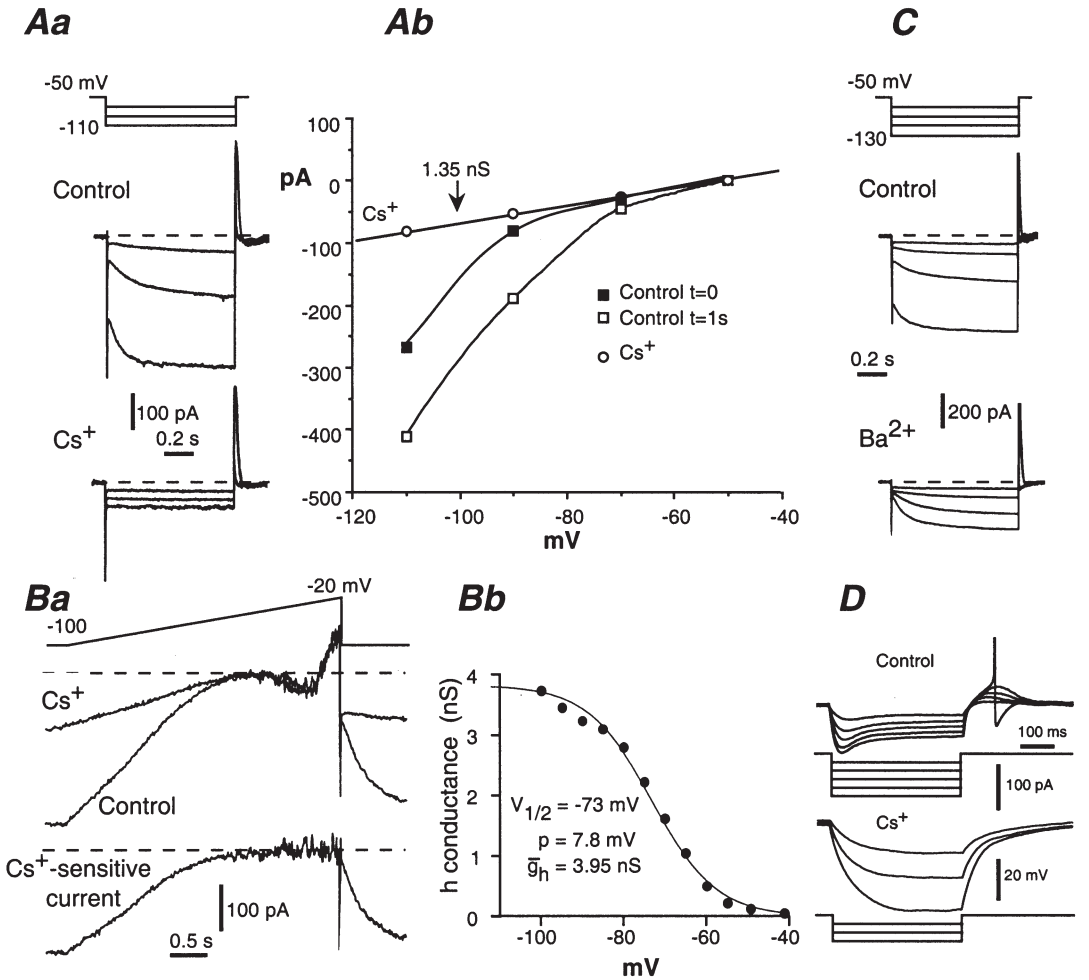

Figure 7. Contribution of I_h to the input conductance of AH neurones

A and *B*, block of I_h with extracellularly applied Cs^+ (2 mM). *Aa*, I_h induced by 1 s hyperpolarizing voltage pulses (incremented by 20 mV). *Ab*, corresponding *I–V* plot. In control conditions, currents were measured at the beginning (filled squares) and at the end (open squares) of the voltage pulse. Cs^+ (circles) blocked both I_h and the inwardly rectifying K^+ current, which is prominent at $V < -90$ mV. *Ba*, currents induced by slowly depolarizing the neurone (16 mV s^{-1}) in control conditions and in the presence of Cs^+. Lower trace, caesium-sensitive current obtained by subtracting the current trace in the presence of Cs^+ to the control current. *Bb*, corresponding voltage dependance of the h conductance. *C*, insensitivity of I_h to Ba^{2+} (2 mM). In contrast to Cs^+, Ba^{2+} did not affect the time-dependent I_h current, but blocked the time-independent inwardly rectifying K^+ current. *D*, current-clamp conditions. Block of I_h with Cs^+ increased the R_{in} of the neurone and abolished the sag in the voltage response to hyperpolarizing current pulses of increasing intensity (20 pA step).

inward current, as demonstrated in Fig. 7*Ba*, which suggests the presence of an inwardly flowing current. This current was insensitive to 0.5 mM Cd^{2+}, indicating that it was not Ca^{2+} dependent, but was probably Na^+ dependent. To isolate this current, part of the Na^+ (125 mM) of the Hepes saline (145 mM Na^+) was replaced with either 125 mM NMDG chloride (Fig. 8*Aa*) or 150 mM choline chloride. The difference current showed that both substitutes strongly decreased I_h and revealed the presence of an inwardly flowing sodium-dependent current present at voltages positive to the I_h activation range (Fig. 8*Ab*). Total blockade of I_h was obtained by adding 1–2 mM Cs^+, which allowed the inwardly flowing sodium-dependent current to be better revealed (Fig. 8*Ba* and *Bb*). This Na^+ current was present in all AH neurones studied ($n = 38$). It had a slow inactivation, the gradual onset of which was revealed by varying the speed of the voltage ramps from 50 to 10 mV s^{-1} (Fig. 8*C*). As a result, slowing the speed decreased the amplitude of the current. This current was voltage dependent. Its threshold was low (around −60 mV). Its peak amplitude was reached between −30 and −20 mV and varied strongly from cell to cell (311 ± 75 pA at 50 mV s^{-1}; $n = 13$). The sodium-dependent current was not affected by a low concentration (100 nM) of TTX,

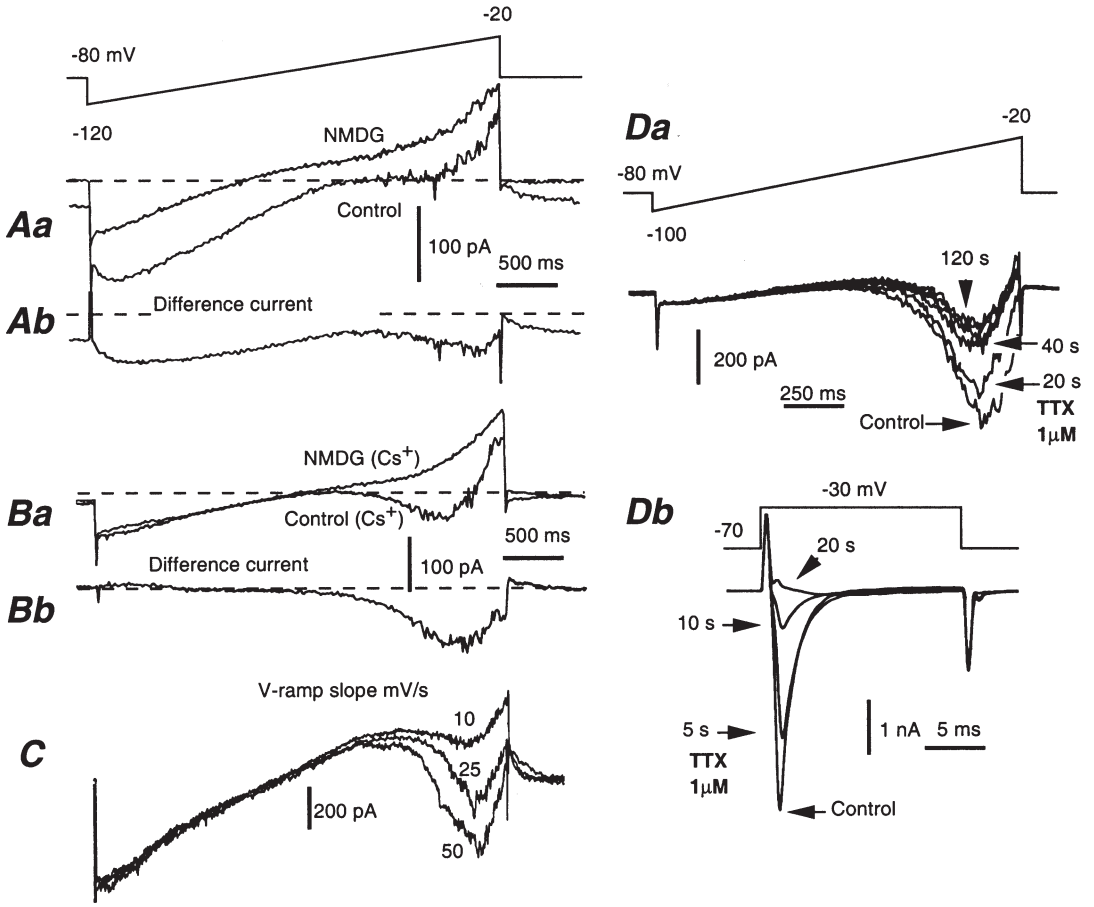

Figure 8. Low-threshold Na^+ current in AH neurones

A and *B*, currents induced by slowly (25 mV s^{-1}) depolarizing AH neurones according to the voltage programme shown in *A*, before (control) and after replacing 90 % of Na^+ by *N*-methyl D-glucamine chloride (NMDG). Lower traces, difference currents showing the sodium-dependent currents. *A*, NMDG strongly depressed I_h and revealed the presence of an inward current at voltages more positive than −50 mV. *B*, same experiment performed in the presence of Cs^+ (2 mM) in order to block I_h. NMDG suppressed a low-threshold, slowly inactivating sodium-dependent current (shown as a difference current *Bb*). This current results in a negative slope conductance in the control *I–V* curve as shown in *Ba*. *C*, AH neurone submitted to voltage ramps at different speeds (50, 25 and 10 mV s^{-1}). As the ramp became slower, the amplitude of the sodium-dependent current decreased as a result of more effective inactivation. *D*, effect of TTX (1 μM) on the slowly inactivating Na^+ current and I_{NaT}. *Da* and *Db*, experiments performed in the presence of 2 mM Cs^+. *Da*, currents induced by depolarizing an AH neurone (40 mV s^{-1}) with voltage ramps from −100 to −20 mV before (control) and 20, 40 and 120 s after bath application of 1 μM TTX. *Db*, current traces of I_{NaT} induced by applying a voltage pulse of 17.5 ms from −70 to −30 mV before (control) and 5, 10 and 20 s after bath application of 1 μM TTX. I_{NaT} was abolished in less than 20 s.

which was sufficient to block the fast-inactivating Na^+ current that participates in the generation of the action potential (I_{NaT}). However, this Na^+-dependent current was attenuated by adding greater concentrations of TTX, 500 nM–2 μM (Fig. 8*Da*). This suggests strongly that there are different populations of Na^+ channels for I_{NaT} and the slowly inactivating Na^+ current. The slowly inactivating, low-threshold sodium-dependent current was absent in S neurones.

Slow I_{AHP}

The I_{AHP} is a slow, time- and voltage-independent, calcium-activated, potassium-selective current that produces the post-action-potential long-lasting hyperpolarization characteristic of AH neurones (Morita *et al.* 1982; Hirst *et al.* 1985*b*). The amplitude of I_{AHP} was strongly dependent on the activation procedure. When I_{AHP} was triggered by a depolarizing pulse, its amplitude and decay time, at a holding potential of −50 mV, increased with the duration of the pulse. Therefore, the presence and amplitude of I_{AHP} were evaluated using a standard protocol. The neurones were subjected to two successive voltage ramps from −120 to 0 mV, spaced 2 s apart (Fig. 9*Aa*). The ramp duration was 5 s. The first ramp induced a Ca^{2+} entry that activated I_{AHP}. This current was obtained by subtracting the current induced by the first ramp from the second (Fig. 9*Ab*). Successive activations of I_{AHP} with voltage pulses or the two-ramp programme resulted in a progressive decline of

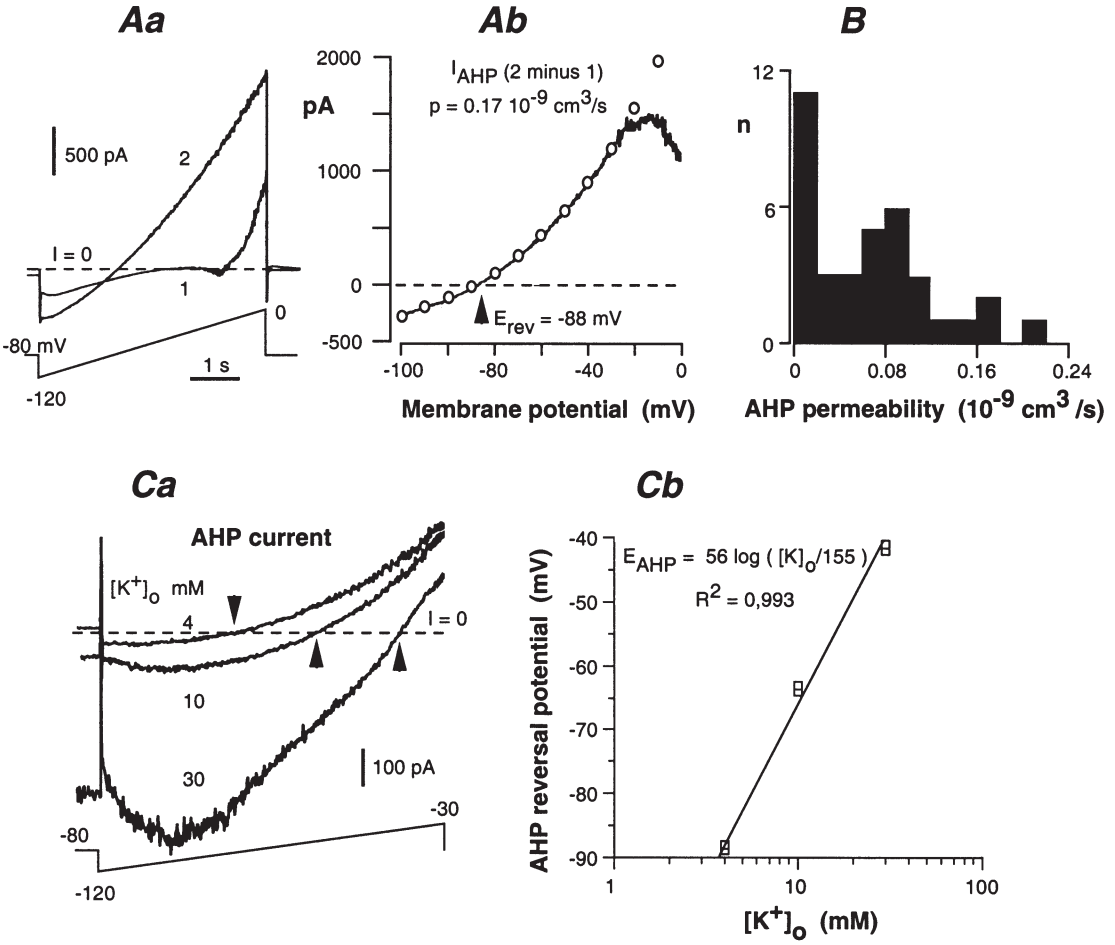

Figure 9. Slow AHP current (I_{AHP}) in AH neurones

A, method for quantifying the slow I_{AHP}. *Aa*, the neurone was depolarized with two successive voltage ramps from −120 to 0 mV separated by 2 s. The first ramp (trace 1) induced a Ca^{2+} entry that activated I_{AHP}, which was prominent in trace 2. *Ab*, I_{AHP} was obtained by subtracting the first current trace from the second. It was fitted to the Goldman-Hodgkin-Katz relationship (open circles) to determine the permeability (*p*). The current decrease that occurred at voltages positive to −20 mV actually resulted from the slow inactivation of the delayed-rectifier K^+ current during the first ramp. *B*, distribution of the AHP permeability in 36 AH neurones. *C*, K^+ dependence of the reversal potential of the AHP current. *Ca*, AHP currents at three different values of $[K^+]_o$. Experiment performed in the presence of 2 mM Cs^+. Arrows indicate the reversal potential of the AHP current. The presence of Cs^+ tended to block the inwardly flowing I_{AHP} in a voltage-dependent manner (i.e. the block increased with the cell polarization). This effect was particularly prominent when the inward I_{AHP} was increased with high $[K^+]_o$. *Cb*, semi-logarithmic plot of the AHP reversal potential versus $[K^+]_o$. Data from two neurones. The straight line has a slope of 56 mV for a 10-fold change in $[K^+]_o$.

the current, presumably by reducing the available intracellular Ca^{2+} pool, which takes part in activating I_{AHP}. Therefore, a 5 min rest period was allowed between two successive activations.

I_{AHP} displayed an outward rectification, as expected from the asymmetrical distribution of K^+ ions. Accordingly, it was well fitted to the Goldman-Hodgkin-Katz (G-H-K) relationship:

$$I = [pVF^2/RT \times ([K^+]_i - [K^+]_o \times \exp(-VF/RT))]/(1 - \exp(-VF/RT)),$$

where R, T, F, $[K^+]_i$ and $[K^+]_o$ (expressed in mmol cm^{-3}) have their usual meaning, and p (in $cm^3\ s^{-1}$) is the AHP-related K^+ permeability of the neurone. In the experiment illustrated in Fig. 9*Ab*, a least-square program led to $p = 0.17 \times 10^{-9}\ cm^3\ s^{-1}$, and $[K^+]_i = 146$ mM. The AHP permeability deduced from the G-H-K relationship displayed large variations, ranging from almost zero (no I_{AHP}) to $0.22 \times 10^{-9}\ cm^3\ s^{-1}$ (Fig. 9*B*).

In physiological saline ($[K^+]_o = 4.8$ mM), I_{AHP} reversed direction at voltages ranging from −86 to −95 mV (−89 ± 1 mV, $n = 16$). The ionic dependence of the I_{AHP} reversal potential was evaluated by changing the K^+ content of the bath saline (Fig. 9*Ca*). These experiments were performed in the presence of 2 mM Cs^+ in order to block the h current, which was itself dependent on $[K^+]_o$ and was prominent in the voltage range where I_{AHP} reversed direction. The plot of the I_{AHP} reversal potential against $\log[K^+]_o$ was linear, with a slope of 56 mV per decade, close to the theoretical value (59 mV) for a K^+ selective current at 35 °C (Fig. 9*Cb*).

All of the above experiments were performed with the standard intracellular saline containing 2 mM EGTA. Although we did not perform a quantitative evaluation, the activation of I_{AHP} was still present when EGTA was replaced with BAPTA and when the concentration of either chelator was increased to 10 mM. The AHP was abolished with 20–40 mM intracellular BAPTA. These facts indicate that the I_{AHP} was highly Ca^{2+} sensitive. This conclusion is consistent with the effects of caffeine that we observed. In order to avoid a muscle Ca^{2+} release and subsequent contractions, caffeine (1 mM) was included in the pipette saline. With 10 mM BAPTA, dialysed caffeine activated an outward current that was detectable within 60 s after breaking the patch (Fig. 10*A*). The current developed progressively while the neurone hyperpolarized (inset in Fig. 10*B*). The activated current had the properties of I_{AHP}: reversal potential near −90 mV and outward rectification (inset in Fig. 10*A*). I_{AHP} peaked after 4–5 min dialysis, and then slowly decreased (Fig. 10*B*), while the neurone depolarized.

Ca^{2+} current in AH neurones

Experiments performed in order to determine the identity of HVA Ca^{2+} channels were made in the presence of the L-type calcium channel blocker nicardipine (3 μM).

In our first series of experiments, we tried to isolate the Ca^{2+} current by perfusing the cells with CsCl (replacing KCl in the patch saline), in order to block outward K^+ currents. This procedure resulted in a large and fast increase in the action potential duration, which lasted up to 3–5 s after a few minutes of dialysis. Under these conditions, however, the cells could not be adequately voltage controlled (i.e. the Ca^{2+} current was triggered in an all-or-none manner).

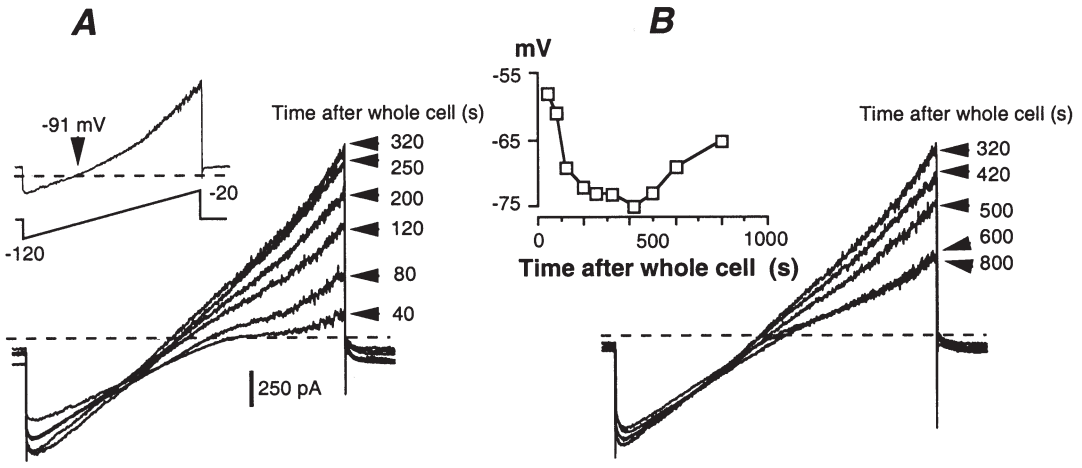

Figure 10. Activation of the slow AHP current with caffeine

Caffeine (1 mM) and 10 mM BAPTA were included in the pipette saline. *A*, progressive activation of I_{AHP} after breaking the patch membrane. I_{AHP} was visualized with successive voltage ramps from −120 to −20 mV. Inset, caffeine-activated current obtained by subtracting the current after 320 s dialysis from the current recorded immediately after breaking the patch membrane ($t = 40$ s). *B*, spontaneous deactivation of the caffeine-induced AHP current. Inset, simultaneous changes in the neurone resting potential measured from the beginning of dialysis.

We therefore used the shape of the action potential to detect the Ca^{2+} current contribution. This contribution was enhanced by adding TEA to the bath. The TEA concentration was set at 10 mM, which resulted in action potentials lasting 30–50 ms (Fig. 11). The highly specific blocker of N-type Ca^{2+} channels, ω-conotoxin GVIA (ω-CgTX GVIA) at 0.5 μM progressively decreased the action potential duration in less than 60 s (Fig. 11*Ab*). The same effect was obtained with another N-type channel blocker, ω-CgTX MVIIA (0.5 μM) (Fig. 11*Bc*). With both blockers present, a hump persisted, indicating a residual Ca^{2+} current. This residual current was eliminated by 0.5 mM Cd^{2+} (Fig. 11*Bc*). This hump was not affected by the P/Q- and N-type channel blocker ω-CgTX MVIIC (0.3–0.5 μM), added with the other toxins present (Fig. 11*Ac* and *Bc*). This blocker, however, had the same effect on the TEA prolonged action potential as ω-CgTX GVIA and MVIIA (Fig. 11*Bb*), although its effect was very fast (steady-state blockade within 15 s at 0.3 μM). Here again, the current resistant to ω-CgTX MVIIC was not affected by the other blockers. The P/Q-type channel blocker ω-aga IVA (0.2 μM) had no effect on the TEA-induced prolongation of action potentials. The lack of additivity between the various blockers indicated that they acted on the same pool of Ca^{2+} channels. The high specificity of ω-CgTX GVIA suggests strongly that these channels are mainly of the N-type.

I_{AHP}, which in the present study was evaluated using the two-ramp method, was blocked by each of the three ω-conotoxins (Fig. 12*A*) with the same time course as the decrease in action potential duration. Since the ω-CgTX-sensitive Ca^{2+} current was investigated mainly in TEA-treated neurones, the same experiments were performed in the presence of 10 mM TEA. By itself, TEA did not prevent I_{AHP} activation by either the voltage-ramp method described above or in response to spiking activity. It reduced, however, the peak of the fast AHP from -70.2 ± 1.5 mV to -66 ± 2 mV with 5 mM TEA, and to

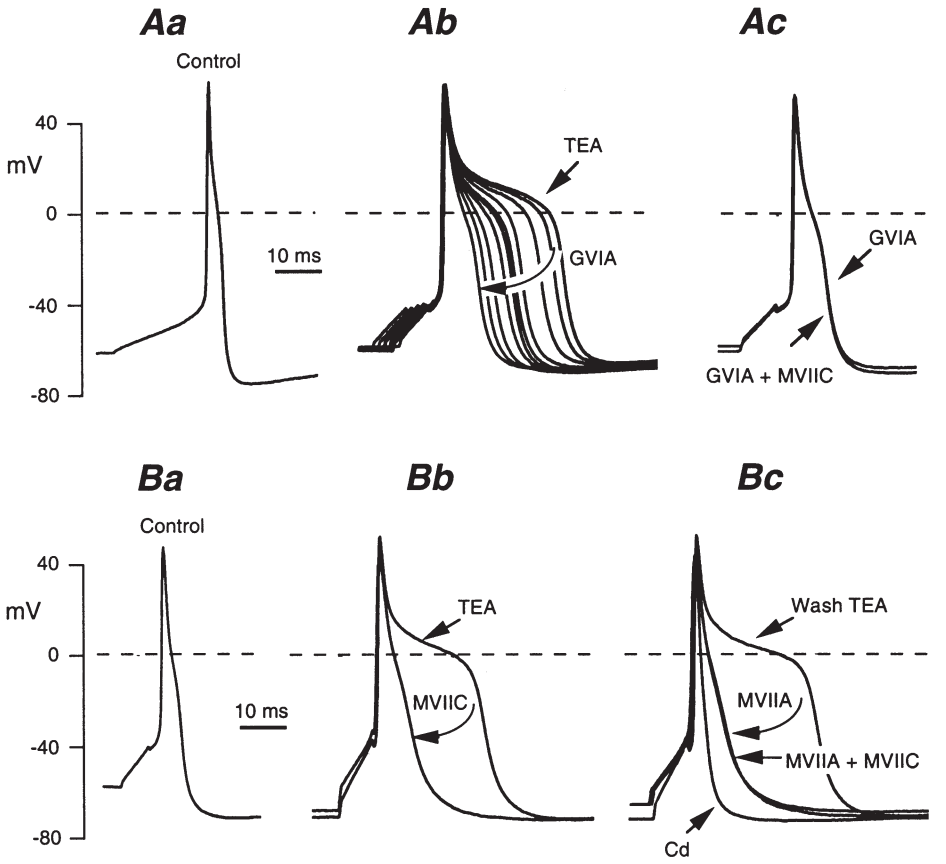

Figure 11. Pharmacological identification of Ca^{2+} current of AH neurones

All experiments were performed in the presence of the L-type Ca^{2+} channels blocker nicardipine (3 μM). *A*, action potentials recorded in control saline (*Aa*), and after adding 10 mM TEA (*Ab*). The elongated TEA-treated action potential was progressively shortened in the presence of ω-conotoxin (ω-CgTX) GVIA (0.5 μM) over a period of 80 s (*Ab*). Adding ω-CgTX MVIIC (0.5 μM) to the ω-CgTX GVIA-containing saline had no additional effect on the action potential shape (*Ac*). *B*, same type of experiment using first ω-CgTX MVIIC (*Bb*), then ω-CgTX MVIIA (0.5 μM) after a 5 min wash period with the TEA saline (*Bc*), and finally ω-CgTX MVIIA plus ω-CgTX MVIIC (*Bc*). At the end of the experiment, the ω-CgTX-resistant action potential elongation was abolished with 0.5 mM Cd^{2+}.

−63.4 ± 1.2 mV with 10 mM TEA (n = 13). These results are in agreement with those of Hirst *et al.* (1985*b*). The enhanced action potentials of TEA-treated neurones were followed by a large AHP, which reached −85 mV (Fig. 12*Bb*). Therefore, I_{AHP} appeared to be poorly TEA-sensitive, at least at the concentrations used here. Even in the presence of TEA to maximize the involvement of the ω-CgTX-resistant Ca^{2+} current, the three ω-conotoxins fully blocked I_{AHP} (Fig. 12*Bc*). Therefore, the ω-CgTX-resistant Ca^{2+} current did not appear to trigger I_{AHP}.

DISCUSSION

In this work we have evaluated the electrophysiological properties of myenteric neurones using the patch-clamp method applied to non-dissociated neurones within intact ganglia of a myenteric plexus/longitudinal muscle preparation.

AH neurones had relatively broad action potentials with a mean half width of 2.8 ms. This figure compares well with those obtained with sharp electrodes: 2.8 ms in the duodenum (Clerc *et al.* 1998) and 2.1–2.7 ms in the ileum (Hirst *et al.* 1985*b*; Iyer *et al.* 1988; Brookes *et al.* 1995). The falling phase of the action potential consistently exhibited a hump (Clerc *et al.* 1998). Two inward currents have been shown to underlie the action potential in the soma, I_{NaT} and a Ca^{2+} current (Hirst *et al.* 1974 ; Hirst *et al.* 1985*a*). A significant difference from the published values, which were obtained with intracellular electrodes, concerns the action potential amplitude measured from the resting potential, 102 mV in this work compared to 72 mV in the duodenum (Clerc *et al.* 1998) and 71–87 mV in the ileum (Hirst *et al.* 1985*b*; Iyer *et al.* 1988; Brookes *et al.* 1995).

A similar observation applied to S neurones. The mean action potential amplitude we measured from the resting potential was 73 mV. Values derived from intracellular recordings ranged from 56 to 65 mV in the duodenum (Clerc *et al.* 1998) and 68 mV in the ileum (Iyer *et al.* 1988).

In view of the greater spike amplitude and of the larger R_{in} (see below), it was expected that patch electrodes would record a more hyperpolarized potential than sharp electrodes. The voltage recorded with patch electrodes is affected by a liquid-junction potential that is due to the low ionic strength of the pipette saline. According to Barry & Lynch (1991), the theoretical junction potential derived from absolute ionic mobilities of the pipette saline would be +4 to +5 mV. This evaluation underestimates the actual shift in voltage when the membrane patch is ruptured, since the cell interior contains large immobile anions. A direct comparison between the recordings of sympathetic neurones performed simultaneously with both types of electrode revealed a junction potential of +9 mV (Gola & Niel, 1993). Substraction of this value gives a mean resting potential of −66 mV for AH and −56 mV for S neurones.

R_{in} was substantially greater with patch electrodes compared to sharp electrodes, which confirms direct comparisons made in isolated myenteric neurones by Baidan *et al.* (1992*a*), who found that the R_{in} of a mixed sample of AH and S neurones was 1010 MΩ with patch electrodes and 111 MΩ with sharp electrodes. In AH neurones in intact ganglia we recorded an R_{in} of 502 MΩ,

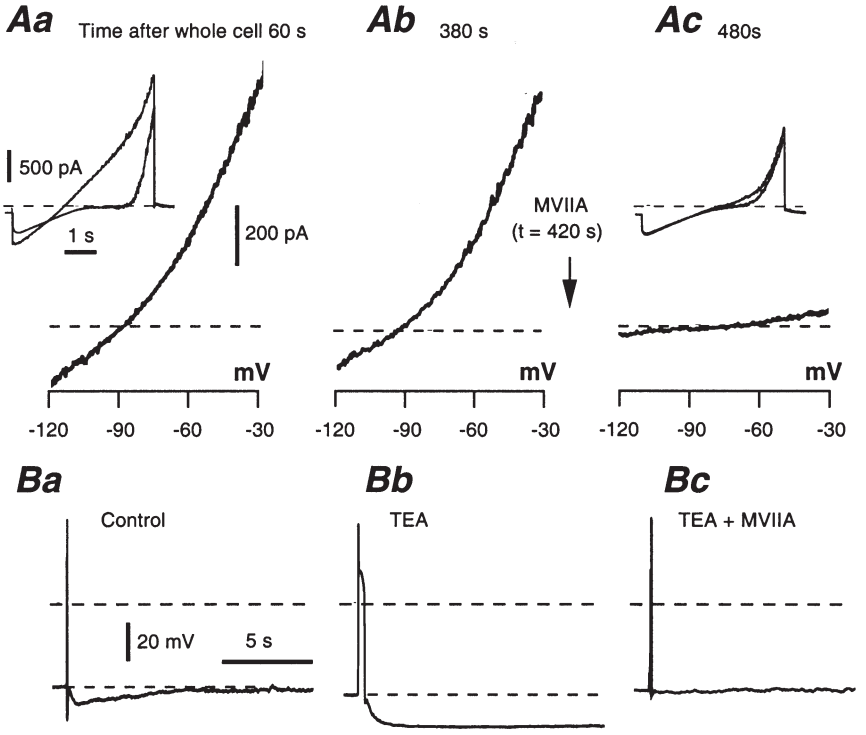

Figure 12. Block of the slow I_{AHP} with ω-CgTX MVIIA

A, I_{AHP} recorded as a difference current in an AH neurone 60 s (*Aa*) and 380 s (*Ab*) after breaking the membrane patch. Inset in *Aa*: two-ramp method applied from −120 to 0 mV. These successive controls were performed systematically to detect a possible spontaneous decrease in I_{AHP}. *Ac*, same protocol applied 60 s after adding 0.5 μM ω-CgTX MVIIA, which abolished I_{AHP}. *B*, effect of 0.5 μM ω-CgTX MVIIA on the slow AHP following the elongation of the action potential with TEA (10 mM). The slow AHP was abolished.

compared with average values of 92–190 MΩ with sharp electrodes in intact ganglia (Hodgkiss & Lees, 1983; Iyer *et al.* 1988; Christofi & Wood, 1994; Kunze *et al.* 1994; Brookes *et al.* 1995; Smith *et al.* 1999). Average values for S neurones in the guinea pig small intestine, recorded with intracellular electrodes, range from about 150 to 350 MΩ (Hodgkiss & Lees, 1983; Iyer *et al.* 1988; Bornstein *et al.* 1991; Kunze *et al.* 1994; Smith *et al.* 1999), although particular subgroups of neurones have different values, for example, longitudinal muscle motor neurones, which have very small cell bodies, have an R_{in} of over 500 MΩ (Smith *et al.* 1999). The value we obtained as an average over all S neurones, 713 MΩ, is 2–3 times the values measured with intracellular electrodes.

I_h was originally observed in guinea-pig AH myenteric neurones by Galligan *et al.* (1990) using a single-electrode voltage-clamp device. These authors found a half-activation at −85 mV and a voltage sensitivity of 10 mV. These values compare well with our data (half activation, −72 mV and voltage sensitivity, 8.2 mV) when the junction potential mentioned above is taken into consideration. The kinetics of activation and deactivation of I_h are strongly voltage dependent. Compared to the h-type currents described in several other cell types (Pape, 1996), I_h in AH neurones has relatively fast on/off kinetics.

In cultured myenteric neurones, Zholos *et al.* (1999) observed a time-dependent current activated by hyperpolarization, which closely resembles the I_h described here, particularly with regard to its kinetics. They ascribed this current to the activation of an inwardly rectifying K^+ conductance. However, I_{Kir} are instantaneously activated by hyperpolarizing pulses. In addition, they are fully blocked by 2 mM Ba^{2+}, whereas the current observed by Zholos *et al.* (1999) persisted in 5 mM Ba^{2+}, although it was slightly decreased (see Pape, 1996, as well as our data for the effect of Ba^{2+} on I_h). The following observations support our identification of the current as I_h. First, I_h was present at the cell resting potential (i.e. at voltages much more positive than E_K; −90 mV in standard conditions: see I_{AHP} section). Second, reducing $[K^+]_o$ from 5 to 2 mM did not affect the location of the activation curve, although it greatly reduced the size of the slowly activating component. Third, the sag in the voltage response to small current pulses appeared at voltages positive to E_K, which could not be accounted for by a K_{ir} current. Together, these data lead us to conclude that in addition to I_{Kir}, *in situ* as well as in culture, AH neurones do express I_h.

Blockade of I_h did not affect the resting membrane potential of AH neurones. This is in agreement with the data of Kilb & Luhmann (2000) obtained in the rat neocortex. As suggested by Galligan *et al.* (1990), the I_h contribution to the input conductance of AH neurones probably accounts for the relatively limited hyperpolarization upon activation of the slow I_{AHP}. In our experiments, this is supported by the fact that even when a large I_{AHP} was generated under voltage-clamp conditions, the AHP of the unclamped cells barely reached −80 mV, although the reversal potential of K^+ ions was at −90 mV.

Our data provide evidence for the presence of an inward current activated from −60 mV in the myenteric sensory neurones. This current appears to be Na^+ dependent because it was suppressed in the presence of NMDG. In addition, it was partly blocked by high concentrations of TTX (500 nM to 2 μM). The remaining current was not Ca^{2+} dependent because it persisted in the presence of Cd^{2+}. In rat suprachiasmatic neurones, a low-threshold, partially TTX-resistant, inward current has also been described (Pennartz *et al.* 1997). The reduction in this low-threshold component of Na^+ current when using slow instead of fast ramps suggests the involvement of a slowly inactivating rather than a persistent Na^+ current (see Pennartz *et al.* 1997). Further experiments are needed to investigate the kinetics of this current. Persistent TTX-sensitive Na^+ currents with voltage dependence similar to that described here have been observed in several preparations (Crill, 1996). Interestingly, as we observed, they were enhanced or presumably unmasked by increasing $[K^+]_o$ (Somjen & Müller, 2000). It is possible that the low-threshold Na^+ current identified in the present study is modulated by second-messenger systems, which might therefore affect neuronal excitability. Recently, such a modulation has been demonstrated to operate on a persistent Na^+ current that was observed in the pyramidal neurones of the rat neocortex (Franceschetti *et al.* 2000).

The physiological significance of the inward rectifier observed in both S and AH neurones is not straightforward to deduce. Myenteric S neurones have a low resting potential, and receive mainly excitatory synaptic inputs. Therefore, S neurones have a low probability to enter the voltage region (around −90 mV) in which the inward rectifier may operate. This region corresponds to the limited window, positive to E_K, which allows K^+ ions to leave the cell. In the case of AH neurones, it can be hypothesized that I_{Kir} may act in synergy with I_{AHP} to clamp the cell at a large polarization. This requires, however, a parallel reduction of I_h. Under these conditions, AH neurones would generate a long-lasting, almost permanent AHP, contributing to the low excitability state that AH neurones may enter. Although this idea has been put forward by Zholos *et al.* (1999), it still needs to be evaluated experimentally.

I_{AHP} was highly variable in size and duration. A direct modulation of calcium-dependent K^+ channels is possible. However, this variation is probably due to variations in $[Ca^{2+}]$. We have shown directly that the I_{AHP} amplitude progressively increased with the release of Ca^{2+} from intracellular stores by dialysing the neurone with 1 mM

caffeine in the presence of a high concentration of BAPTA. In addition, a mechanism underlying the modulation of I_{AHP} expression might be the blockade of Ca^{2+} channels upon synaptic activation, as has been suggested by Grafe *et al.* (1980).

Our data provide an unequivocal identification of HVA Ca^{2+} channels that activate the calcium-dependent K^+ conductance that underlies the AHP. The absence of an effect of ω-aga IVA on the action potential shows that these channels are not of the P/Q type, although Starodub & Wood (1999) suggested the existence of a P/Q-type current in cultured myenteric neurones. The strong decrease in duration of the action potential in the presence of ω-CgTX GVIA and MVIIA, which have a high affinity for N-type channels, was never accentuated by adding ω-CgTX MVIIC, which blocks both N- and P/Q-type channels. However, a small Ca^{2+} component of the action potential was resistant to all of the toxins. This suggests strongly that most of the HVA channels in guinea-pig myenteric sensory neurones belong to the N type. Abolition of the AHP with ω-CgTX MVIIA demonstrated that N-type channels are the unique HVA Ca^{2+} channels, whose opening triggers the AHP, although a minor contribution of other HVA Ca^{2+} channels was suggested by previous data (Vogalis *et al.* 2001). This conclusion is strengthened by the fact that, in our experiments, the toxin was capable of blocking an AHP that was exaggerated by using 10 mM TEA to increase Ca^{2+} influx during the action potential. Our conclusion is consistent with the observation that myenteric sensory neurones express a high level of immunoreactivity to the α1 subunits of class B (N-type) but not of class A channels (P/Q-type; Kirchgessner & Liu, 1999).

In conclusion, our results extend knowledge of the types of currents expressed in the myenteric sensory neurones of the guinea-pig. We have shown that I_h is a major conductance of myenteric sensory neurones, despite the fact that this conductance was not recognized in a recent patch study. In addition, we have discovered the presence of a low-threshold sodium-dependent current that is poorly sensitive to TTX. Finally, we have provided unambiguous evidence that N-type Ca^{2+} channels are the unique HVA channels that trigger the AHP.

REFERENCES

Baidan, L. V., Zholos, A. V., Shuba, M. F. & Wood, J. D. (1992*a*). Patch-clamp recording in myenteric neurones of guinea-pig small intestine. *American Journal of Physiology* **262**, G1074–1078.

Baidan, L. V., Zholos, A. V. & Wood, J. D. (1992*b*). Properties of calcium currents determined by patch-clamp recording in myenteric neurones from adult guinea-pig small intestine. *Gastroenterology* **102**, A420.

Barry, P. H. & Lynch, J. W. (1991). Liquid junction potentials and small cell effects in patch-clamp analysis. *Journal of Membrane Biology* **121**, 101–117.

Bornstein, J. C., Costa, M., Furness, J. B. & Lees, G. M. (1984). Electrophysiology and enkephalin immunoreactivity of identified myenteric plexus neurones of guinea-pig small intestine. *Journal of Physiology* **351**, 313–325.

Bornstein, J. C., Furness, J. B., Smith, T. K. & Trussell, D. C. (1991). Synaptic responses evoked by mechanical stimulation of the mucosa in morphologically characterized myenteric neurons of the guinea-pig ileum. *Journal of Neuroscience* **11**, 505–518.

Bornstein, J. C., Furness, J. B. & Kunze, W. A. A. (1994). Electrophysiological characterization of myenteric neurons: how do classification schemes relate? *Journal of the Autonomic Nervous System* **48**, 1–15.

Brookes, S. J. H., Song, Z. M., Ramsay, G. A. & Costa, M. (1995). Long aboral projections of Dogiel type II, AH neurons within the myenteric plexus of the guinea pig small intestine. *Journal of Neuroscience* **15**, 4013–4022.

Christofi, F. L. & Wood, J. D. (1994). Electrophysiological subtypes of inhibitory P1 purinoceptors on myenteric neurones of guinea-pig small bowel. *British Journal of Pharmacology* **113**, 703–710.

Clerc, N., Furness, J. B., Bornstein, J. C. & Kunze, W. A. A. (1998). Correlation of electrophysiological and morphological characteristics of myenteric neurones of the duodenum in the guinea-pig. *Neuroscience* **82**, 899–914.

Clerc, N., Gola, M., Rugiero, F., Furness, J. B. & Kunze, W. A. A. (2000). Properties of patch clamped myenteric sensory neurons in intact ganglia. *Autonomic Neuroscience: Basic and Clinical* **82**, 65.

Costa, M., Brookes, S. J. H., Steele, P. A., Gibbins, I., Burcher, E. & Kandiah, C. J. (1996). Neurochemical classification of myenteric neurons in the guinea-pig ileum. *Neuroscience* **75**, 949–967.

Crill, W. E. (1996). Persistent sodium current in mammalian central neurons. *Annual Review of Physiology* **58**, 349–362.

Doan, T. N. & Kunze, D. L. (1999). Contribution of the hyperpolarization-activated current to the resting membrane potential of rat nodose sensory neurons. *Journal of Physiology* **514**,125–138.

Franceschetti, S., Taverna, S., Sancini, G., Panzica, F., Lombardi, R. & Avanzini, G. (2000). Protein kinase C-dependent modulation of Na^+ currents increases the excitability of rat neocortical pyramidal neurones. *Journal of Physiology* **528**, 291–304.

Franklin, J. L. & Willard, A. L. (1993). Voltage-dependent sodium and calcium currents of rat myenteric neurones in cell culture. *Journal of Neurophysiology* **69**, 1264–1275.

Furness, J. B. (2000). Types of neurons in the enteric nervous system. *Journal of the Autonomic Nervous System* **81**, 87–96

Furness, J. B., Kunze, W. A. A., Bertrand, P. P., Clerc, N. & Bornstein, J. C. (1998). Intrinsic primary afferent neurones of the intestine. *Progress in Neurobiology* **54**, 1–18.

Galligan, J. J., Tatsumi, H., Shen, K-Z., Surprenant, A. & North, R. A. (1990). Cation current activated by hyperpolarization (I_h) in guinea pig enteric neurones. *American Journal of Physiology* **259**, G966–972.

Gola, M. & Niel, J. P. (1993). Electrical and integrative properties of rabbit sympathetic neurones re-evaluated by patch clamping non-dissociated cells. *Journal of Physiology* **460**, 327–349.

Grafe, P., Mayer, C. J. & Wood, J. D. (1980). Synaptic modulation of calcium-dependent potassium conductance in myenteric neurones in the guinea-pig. *Journal of Physiology* **305**, 235–248.

Hanani, M., Franke, M., Hartig, W., Groshe, J., Reichenbach, A. & Pannicke, T. (2000). Patch-clamp study of neurones and glial cells in isolated myenteric ganglia. *American Journal of Physiology* **278**, G644–651.

Hirst, G. D. S., Holman, M. E. & Spence, I. (1974). Two types of neurones in the myenteric plexus of the duodenum in the guinea-pig. *Journal of Physiology* **236**, 303–326.

Hirst, G. D. S., Johnson, S. M. & van Helden, D. F. (1985*a*). The calcium current in a myenteric neurone of the guinea-pig ileum. *Journal of Physiology* **361**, 297–314.

Hirst, G. D. S., Johnson, S. M. & van Helden, D. F. (1985*b*). The slow calcium-dependant potassium current in a myenteric neurone of the guinea-pig ileum. *Journal of Physiology* **361**, 315–337.

Hodgkiss, J. P. & Lees, G. M. (1983). Morphological studies of electrophysiologically-identified myenteric plexus neurones of the guinea-pig ileum. *Neuroscience* **8**, 593–608.

Iyer, V., Bornstein, J. C., Costa, M., Furness, J. B., Takahashi, Y. & Iwanaga, T. (1988). Electrophysiology of guinea-pig myenteric neurones correlated with immunoreactivity for calcium binding proteins. *Journal of the Autonomic Nervous System* **22**, 141–150.

Johnson, S. M., Katayama, Y., Morita, K. & North. R. A. (1981). Mediators of slow synaptic potentials in the myenteric plexus of the guinea-pig ileum. *Journal of Physiology* **320**, 175–186.

Johnson, S. M., Katayama, Y. & North, R. A. (1980). Slow synaptic potentials in neurones of the myenteric plexus. *Journal of Physiology* **301**, 505–516.

Kilb, W. & Luhmann, H. J. (2000). Characterization of a hyperpolarization-activated inward current in Cajal-Retzius cells in rat neonatal neocortex. *Journal of Neurophysiology* **84**, 1681–1691.

Kirchgessner, A. L. & Liu, M. T. (1999). Differential localization of Ca^{2+} channel alpha 1 subunits in the enteric nervous system; presence of alpha 1B channel-like immunoreactivity in intrinsic primary afferent neurones. *Journal of Comparative Neurology* **409**, 85–104.

Kunze, W. A. A., Bornstein, J. C., Furness, J. B., Hendriks, R. & Stephenson, D. S. H. (1994). Charybdotoxin and iberiotoxin but not apamin abolish the slow after-hyperpolarization in myenteric plexus neurones. *Pflügers Archiv* **428**, 300–306.

Kunze, W. A. A., Clerc, N., Furness, J. B. & Gola, M. (2000). The soma and neurites of primary afferent neurones in the guinea-pig intestine respond differentially to deformation. *Journal of Physiology* **526**, 375–385.

Morita, K., North, R. A. & Tokimasa, T. (1982). The calcium-activated potassium conductance in guinea-pig myenteric neurones. *Journal of Physiology* **329**, 341–354.

Nishi, S. & North, R. A. (1973). Intracellular recording from the myenteric plexus of the guinea-pig ileum. *Journal of Physiology* **231**, 471–491.

Pape, H-C. (1996). Queer current and pacemaker: the hyperpolarization-activated cation current in neurones. *Annual Review of Physiology* **58**, 299–327.

Pennartz, C. M. A., Bierlaagh, M. A. & Geurtsen, A. M. S. (1997). Cellular mechanisms underlying spontaneous firing in rat suprachiasmatic nucleus: involvement of a slowly inactivating component of sodium current. *Journal of Neurophysiology* **78**, 1811–1825.

Smith, T. K., Burke, E. P. & Shuttleworth, C. W. (1999). Topographical and electrophysiological characteristics of highly excitable S neurones in the myenteric plexus of the guinea-pig ileum. *Journal of Physiology* **517**, 817–830.

Somjen, G. G. & Müller M. (2000). Potassium-induced enhancement of persistent inward current in hippocampal neurons in isolation and in tissue slices. *Brain Research* **885**, 102–110.

Song, A. M., Brookes, S. J. H., Ramsay, G. A. & Costa, M. (1997). Characterization of myenteric interneurons with somatostatin immunoreactivity in the guinea-pig small intestine. *Neuroscience* **80**, 907–923.

Starodub, A. M. & Wood, J. D. (1999). Selectivity of omega-CgTx-MVIIC toxin from Conus magnus on calcium currents in enteric neurones. *Life Science* **64**, PL305–310.

Starodub, A. M. & Wood, J. D. (2000). A-type potassium current in myenteric neurons from guinea pig small intestine. *Neuroscience* **99**, 389–396.

Uchitel, O. D. (1997). Toxins affecting calcium channels in neurones. *Toxicon* **35**, 1161–1191.

Vogalis, F., Hillsley, K. & Smith, T. K. (2000). Diverse ionic currents and electrical activity of cultured myenteric neurones from the guinea pig proximal colon. *Journal of Neurophysiology* **83**, 1253–1263.

Vogalis, F., Furness, J. B. & Kunze, W. A. A. (2001). Afterhyperpolarization current in myenteric neurons of the guinea pig duodenum. *Journal of Neurophysiology* **85**, 1941–1951.

Wood, J. D. & Meyer, C. J. (1978). Intracellular study of electrical activity of Auerbach's plexus in guinea-pig small intestine. *Pflügers Archiv* **374**, 265–275.

Zholos, A. V., Baidan, L. V., Starodub, A. M. & Wood, J. D. (1999). Potassium channels of myenteric neurones in guinea-pig small intestine. *Neuroscience* **89**, 603–618.

Acknowledgements

This work was supported by the Centre National de la Recherche Scientifique (CNRS, France), the National Health and Medical Research Council of Australia (grant 96323) and by Australia-France exchange grants from the Programme International de Coopération Scientifique (PICS, France) and the International Researcher Exchange Scheme (IREX, Australian Research Council).